electronics

Article

An Angle-Stable Ultra-Wideband Single-Layer Frequency Selective Surface Absorber

Chonghuan Zhang, Siyuan Liu, Haizhi Ni, Renxuan Tan, Changjun Liu and Liping Yan *

College of Electronics and Information Engineering, Sichuan University, Chengdu 610065, China; zch@stu.scu.edu.cn (C.Z.); tanrenxuan@stu.scu.edu.cn (R.T.); cjliu@scu.edu.cn (C.L.)
* Correspondence: liping_yan@scu.edu.cn

Abstract: An ultra-wideband polarization-insensitive frequency selective surface (FSS) absorber is proposed for S to K-band applications. The absorber comprises two compensation slabs, a lossy FSS layer and a grounded dielectric plate. The FSS unit cell is a combination of a second-order Chinese knot and a cross. To enhance the bandwidth and angular stability of the single-layer FSS absorber, a compensation layer composed of FR4 and polymethyl methacrylate (PMMA) slabs is incorporated. The proposed FSS absorber demonstrates a remarkable absorption rate of over 90% within the frequency range of 3.1–22.1 GHz, exhibiting a fractional bandwidth of 150.8%. Even when subjected to an oblique incidence of 45°, the absorber maintains an 80% absorption rate in the frequency range of 4.4–19.1 GHz for both TE and TM polarizations. The total thickness of the FSS absorber is 0.0848 λ_L (the wavelength at the lowest cutoff frequency), and only 1.08 times the Rozanov limit. To validate the design, a prototype of the proposed absorber was fabricated and measured. Good agreements were observed between the simulations and measurements.

Keywords: absorber; frequency selective surface; single-layer; thin; ultra-wideband

Citation: Zhang, C.; Liu, S.; Ni, H.; Tan, R.; Liu, C.; Yan, L. An Angle-Stable Ultra-Wideband Single-Layer Frequency Selective Surface Absorber. *Electronics* **2023**, *12*, 3776. https://doi.org/10.3390/electronics12183776

Academic Editor: Antonio Orlandi

Received: 10 August 2023
Revised: 31 August 2023
Accepted: 4 September 2023
Published: 7 September 2023

1. Introduction

Frequency selective surface (FSS) absorbers offer several advantages over traditional electromagnetic wave absorbing materials and structures, including a low profile, broadband absorption [1] and a flexible structural design [2]. Consequently, they have found extensive application in various fields such as radar cross-section reduction (RCS) [3,4], electromagnetic interference suppression [5–7], antenna gain enhancement [8], and stealth technology [9]. The continuous advancements in radar and wireless technologies have sparked researchers' interest in developing FSS absorbers with ultra-broadband capability, high angle stability, ultra-thinness, and strong absorption.

Multi-layer FSS structures are commonly utilized in the design of ultra-wideband FSS absorbers [10–12]. For example, Zheng et al. [10] proposed a three-layer FSS absorber that achieves a 90% absorption bandwidth ranging from 2.2 GHz to 18 GHz (156.4%), with a thickness of 0.088 λ_L (wavelength at the lowest frequency). It also demonstrates angular stability of 40° for TE polarization and 60° for TM polarization. Another three-layer FSS absorber designed by Gao et al. [11] exhibits a 90% absorption bandwidth covering 2 GHz to 23 GHz (168%) and maintains absorption levels exceeding 90% at 45° oblique incidence, with a thickness of 0.1 λ_L. Additionally, Sun et al. [12] successfully created a two-layer FSS absorber with a 90% absorption band of 2.79–20.62 GHz (152%). It possesses a thickness of 0.115 λ_L and offers angular stability of up to 60° for both TE and TM polarizations. However, the design of multi-layer FSS absorbers is challenging, and there is a risk of performance degradation in practical applications due to alignment errors between the FSS units in each layer, especially when the period of each layer varies.

Single-layer FSS absorbers can effectively address these issues. The combination of multi-resonant structures and compensation dielectric slabs have gained popularity [13–17] in the design of wideband single-layer FSS absorbers. Cao et al. [13] proposed an ultra-broadband single-layer FSS absorber using the novel concept of an “impedance well”. This absorber incorporates 16 lumped elements in each unit cell and achieves a 90% absorption band from 0.45 GHz to 2.34 GHz (135.5%). Sheokand et al. [14] presented a resistive film FSS absorber that utilizes interdigital capacitance with a square ring and four patches. This design provides over 90% absorption in the frequency range of 4–17.2 GHz, with a thickness of $0.08\lambda_L$ and an 80% absorption angular stability of up to 40°. He et al. [15] introduced a FSS absorber with two dielectric compensation layers to enhance its bandwidth. This absorber achieves a 90% absorption bandwidth from 2.3 GHz to 13.3 GHz (141.0%), with an angular stability of up to 45°, albeit with a relatively higher thickness of $0.138\lambda_L$. By replacing the lossless compensation layers with a patterned lossy light honeycomb layer, the bandwidth of the absorber is extended to 2.89–18.0 GHz (144.7%) [16]. Furthermore, Zhao et al. designed an optically transparent flexible absorber using a single-layer FSS and a single-layer dielectric compensation layer [17]. This absorber achieves a 90% absorption bandwidth of 135.5% (5.61–29.17 GHz), with an angular stability of 30° and 60° for TE and TM polarizations, respectively. While ferromagnetic materials have shown promise in designing ultra-broadband ultra-thin broadband FSS absorbers [18], their high density and dispersive electromagnetic characteristics limit their applications. Thus, it is still a great challenge to design ultra-wideband angle-stable thin absorbers by using only single-layer FSS structures.

In this paper, an ultra-wideband thin absorber based on a single-layer indium tin oxide (ITO) FSS is proposed. The miniaturized FSS unit cell consists of a second-order Chinese knot combined with a cross, enabling multiple current paths and achieving impedance matching across a wide frequency range. To enhance bandwidth and oblique incident angle stability, a compensation layer composed of FR4 and polymethyl methacrylate (PMMA) slabs was incorporated. The proposed FSS absorber demonstrates over 90% absorption in the range of 3.1–22.1 GHz (150.8%) for normal incidence. Even at an incident angle of 45°, the absorber retains over 80% absorption in the range of 4.4–19.1 GHz for both TE and TM polarizations. Moreover, the thickness of the absorber is only $0.0848\lambda_L$, approximately 1.08 times the Rozanov limit [19]. Finally, a prototype was fabricated and measured. Good agreements between the simulations and measurements were observed.

This paper is organized as follows: the design evolution and analysis of the proposed absorber is presented in Section 2, followed by its performance evaluation in Section 3, where incident angle stability and the effects of sheet resistance fluctuation on the performance of the absorber are explored. The physical experiment is implemented for validation of simulation results in Section 4. Finally, the conclusion is drawn in Section 5.

2. Design and Analysis of the Absorber

The configuration of the proposed FSS absorber is illustrated in Figure 1. The absorber consisted of several layers including a FR4 dielectric slab, a PMMA slab, a resistive film FSS layer, a polymethacrylimide (PMI) foam, and a metal ground plate. The PMI foam, which had a low relative dielectric constant of 1.06, was positioned between the metal ground and the FSS layer. The meticulously designed FSS layer was constructed using ITO film, with a sheet resistance of 36 Ω/sq. The ITO film was deposited on a substrate made of polyethylene terephthalate (PET), which had a relative dielectric constant of 3 and loss tangent of 0.06. It is worth noting that other types of resistive film with the same sheet resistance can be utilized to fabricate the lossy FSS layer, but ITO is preferred for its commercial availability. In order to ensure angular stability and to improve the bandwidth of the absorber, two additional dielectric slabs were incorporated. The first was a FR4 slab, which possessed a relative dielectric constant of 4.3 and a loss tangent of 0.025. The second was a PMMA slab with a relative dielectric constant of 2.55 and an exceptionally low loss tangent of 0.0002. The strategic arrangement of these layers aimed to optimize the absorbing characteristics of the proposed single-layer FSS absorber while considering factors such as bandwidth enhancement and incident angular stability.

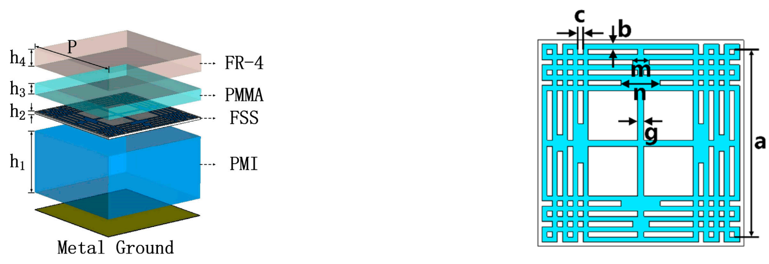

(**a**) (**b**)

Figure 1. The unit cell topology of the proposed FSS absorber: (**a**) unit cell and (**b**) FSS pattern.

2.1. Design of the FSS Unit Cell

To achieve a broadband, angle-stable, and polarization-insensitive FSS absorber, the unit cell pattern must possess characteristics such as miniaturization, 90-degree rotational symmetry, and diverse current paths for multiple resonances in a wide frequency range. Therefore, a folded square ring derived from a one-order Chinese knot combined with a cross was employed as the initial FSS unit cell (shown in Figure 2a). The reflection coefficient and input impedance of the absorber composed of the initial FSS and a grounded PMI foam with thickness of 5.5 mm were simulated using commercial software CST 2019 [20], and the results are illustrated in Figure 2b,c, respectively. The absorption rate can be given as

$$A(f) = \left(1 - |S_{11}|^2 - |S_{21}|^2\right) \times 100\% \quad (1)$$

where $|S_{11}|$ and $|S_{21}|$ are the reflection and transmission coefficients of the absorber. For an absorber grounded with a metal plate, electromagnetic waves cannot transmit through the absorber. Thus, $|S_{11}| < -10$ dB resulted in over 90% absorption, and $|S_{11}| < -7.0$ dB led to over 80% absorption.

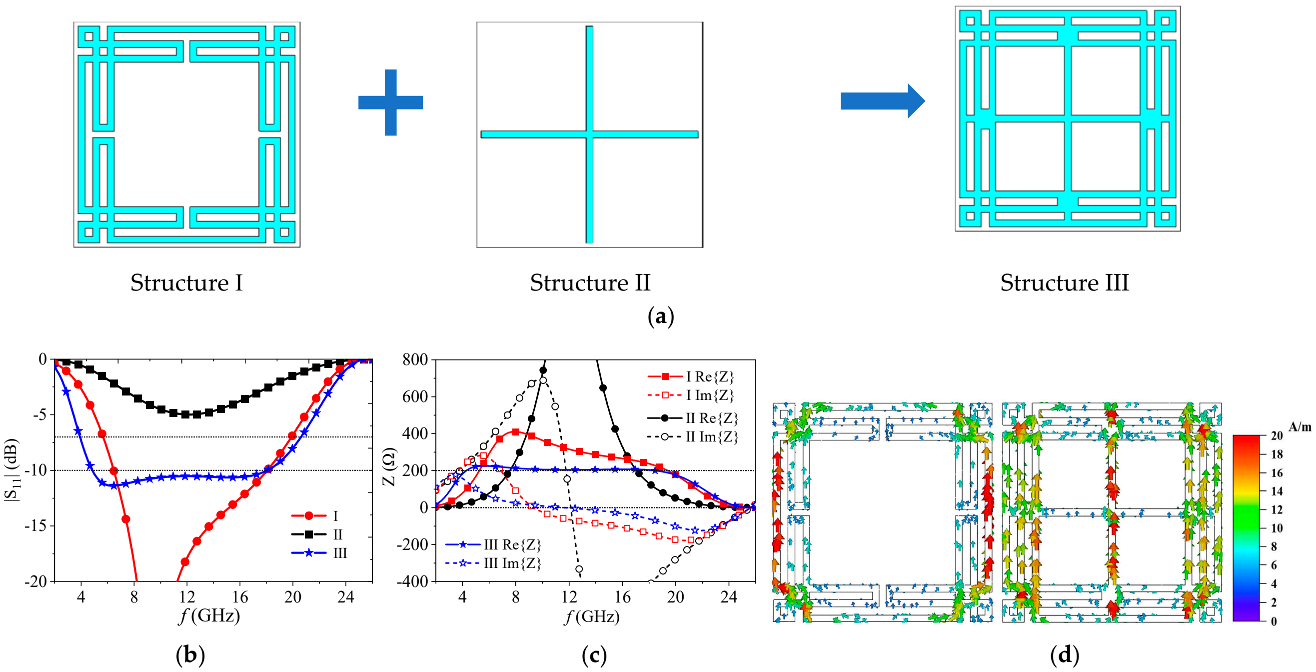

Figure 2. Initial unit cell geometry (**a**). Reflection coefficient (**b**) and input impedance (**c**) of the absorber composed of different FSS structures. Current density distribution at 5 GHz (**d**).

In Figure 2b, the absorber composed of only a one-order Chinese knot (structure I) exhibited a −10 dB bandwidth of (6.5–18.0) GHz (93.9%), while the absorber with the cross (structure II) did not show any resonance within this frequency range. However, combining these two structures (structure III) enhanced the −10 dB bandwidth. This enhancement can be attributed to the impedance variation observed in Figure 2c. For example, the resistance of structure I was initially less than 200 Ω at 5 GHz. However, upon introducing the cross, the resistance increased to approximately 225 Ω, while the reactance decreased to approach zero simultaneously. This variation occurred because the cross pattern not only provided an additional current path at 5 GHz, but also connected the separated branches of the Chinese knot together, as shown in Structure III in Figure 2a. As a result, the induced current distribution along the inner branches of the Chinese knot was enhanced at 5 GHz, as illustrated in Figure 2d. All these current distributions contributed to the impedance variation, improving the impedance matching at 5 GHz.

Figure 3 provides the reflection coefficient of the absorber composed of FSS structure III at different incident angles (θ). In the case of TE polarization, as the incident angle θ increases, the reflection coefficient also increased, accompanied by a slight shift in the frequency band, as shown in Figure 3a. However, for TM polarization, the −10 dB bandwidth significantly shifted to higher frequencies, as depicted in Figure 3b. This shift was caused by the changes in both the input impedance and wave impedance in free space, which became 377 Ω/cosθ for TE and 377 Ω·cosθ for TM polarizations, respectively [21]. For TE polarization, the input impedance remained almost unchanged in terms of its real part with respect to the incident angle θ in the frequency range below 16 GHz. However, its imaginary part gradually increased, as shown in Figure 4a, leading to an increase in the reflection coefficient. On the other hand, for TM polarization, both the real and imaginary parts of the input impedance varied with the incident angle θ, but in an opposite manner in the frequency range below 18 GHz, as illustrated in Figure 4b.

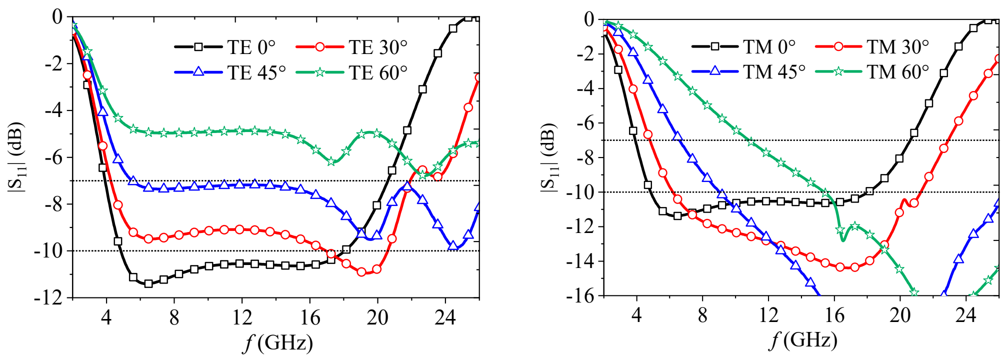

(**a**) (**b**)

Figure 3. Reflection coefficient of the structure III with respect to incident angles for (**a**) TE and (**b**) TM polarizations.

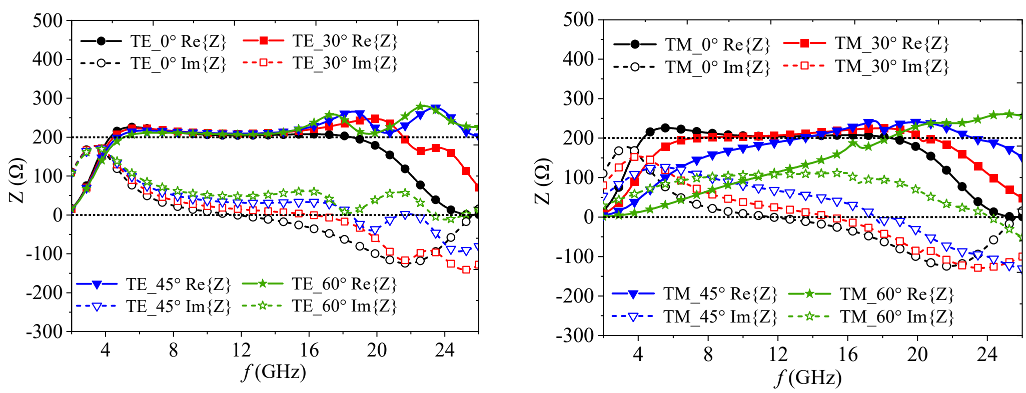

(**a**) (**b**)

Figure 4. Input impedance of the structure III with respect to incident angles for (**a**) TE and (**b**) TM polarizations.

2.2. Design of the Compensation Layer

To improve angular stability and further enhance the bandwidth of the initial absorber (structure III), a compensation dielectric slab was introduced on top of the absorber. This compensation layer can be considered as an impedance matching layer, and thus its thickness (h_s) was determined according to the cancellation of reflections from its two interfaces A and B, as shown in Figure 5a. The thickness of the slab is thus given as

$$h_s = \frac{\lambda_0}{4} \frac{1}{\sqrt{\varepsilon_r - sin^2\theta}} \tag{2}$$

where λ_0 is the center frequency of the interested band, and ε_r is the relative dielectric constant of the slab. Here, a FR4 substrate was chosen as the compensation slab, with an interested frequency band of (4.0–24.0) GHz. Thus, the thickness of the slab was calculated as h_s = 2.75 mm, but for fabrication tolerance and overall thickness consideration, a 2.5 mm-thick FR4 slab was used as the compensation layer. However, when the compensation layer was introduced, the reflection coefficient of the FSS absorber (shown in Figure 5b) became larger than −10 dB in the frequency range from 10.1 GHz to 19.6 GHz, resulting in a degradation in absorption. This was due to the fact that the real part of the input impedance dropped below 200 Ω in this frequency range, while the imaginary part only underwent a slight change, as depicted in Figure 5c.

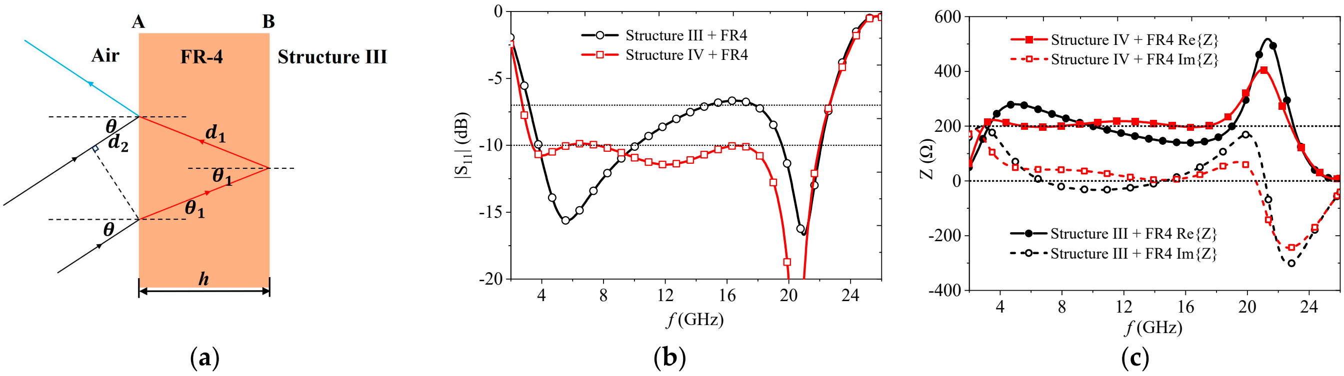

Figure 5. (**a**) Schematic diagram of reflection and transmission of electromagnetic waves, (**b**) the reflection coefficient, and (**c**) input impedance of the whole structure.

To tackle this problem, the real part of the input impedance should be increased. The effective resistance of a resistive film FSS depends on factors such as the unit cell pattern, sheet resistance, and current distribution. Since the impedance matched well outside the frequency range of 10.1–19.6 GHz, a better option for improving impedance matching within this band was to alter the unit cell pattern and, consequently, the current distribution. Therefore, the one-order Chinese knot in the FSS unit cell was modified to a second-order Chinese knot, while the other configuration remains the same (structure IV), as shown in Figure 6a. The reflection coefficient and input impedance of the modified FSS absorber (structure IV + FR4) are presented in Figure 5b,c, respectively. It is evident that the impedance matches well in the frequency range of 3.4–22.0 GHz (146.4%), except for around 6.5 GHz. However, when the incident angle increased to 45°, the reflection coefficient for TE polarization increased beyond −7.0 dB around 20.3 GHz, as illustrated in Figure 6b, thereby reducing the absorption bandwidth of the absorber.

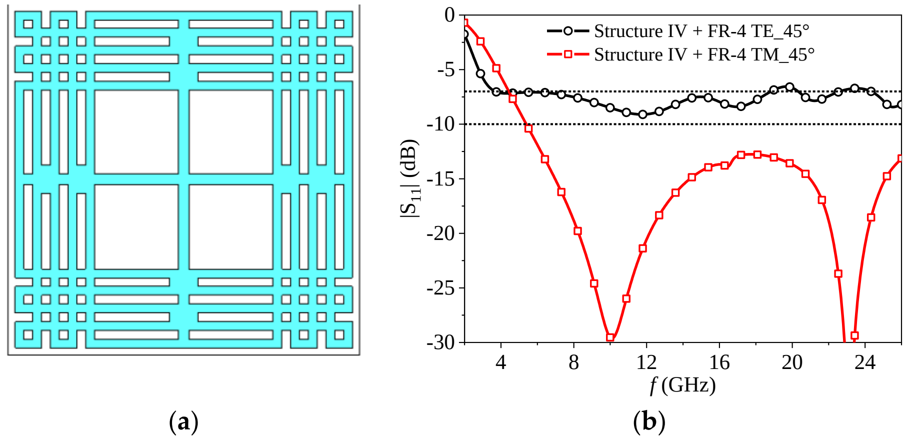

Figure 6. Pattern of the modified FSS (structure IV) (**a**) and reflection coefficient of the modified absorber at incident angle of 45° (**b**).

Without changing the thickness of the compensation layer, only varying the dielectric constant of the compensation slab did not effectively solve these problems, as revealed by Figure 7a,b. Instead, splitting the compensation layer into two slabs with different thickness and dielectric constant was explored, which could introduce additional reflections that cancel each other at the interface of the absorber. By employing a FR4 substrate with a thickness of 1.5 mm as one slab, the dielectric constant of another slab with a thickness of 1 mm was determined by a parameter sweep, and the results are provided in Figure 8a,b. It revealed that a substrate with a dielectric constant of 2.5 can meet the requirements of a broad bandwidth and angular stability. Thus, the PMMA material was chosen as another slab for compensation layer.

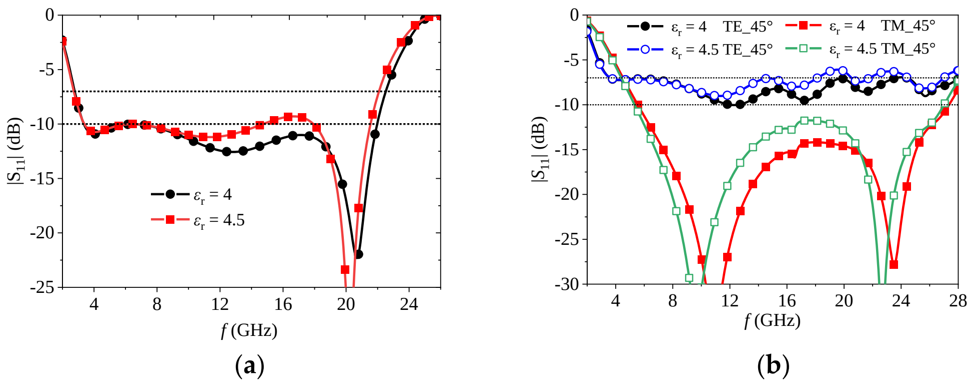

Figure 7. Reflection coefficient of the absorber with only one compensation slab for (**a**) normal incidence and (**b**) oblique incidence at 45°.

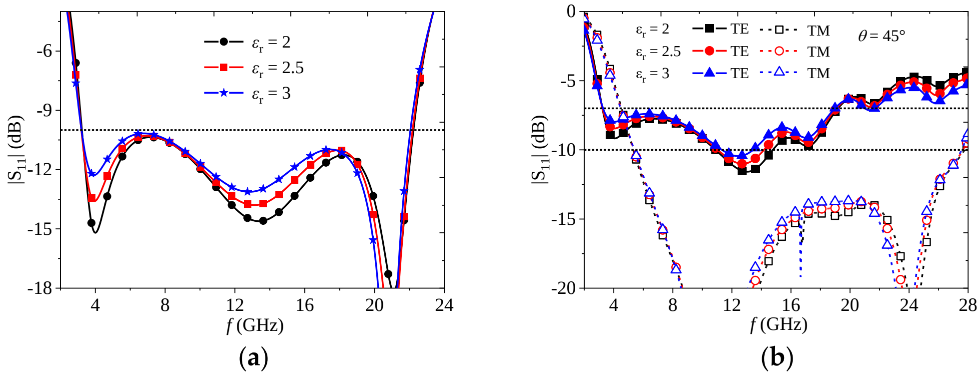

Figure 8. Reflection coefficient of the absorber with two compensation slabs with respect to the dielectric constant of another slab for (**a**) normal incidence and (**b**) oblique incidence at 45°.

2.3. Effects of Patches on the Absorber

The rectangular patches formed where the second-order Chinese knot meet the cross. The effects of these patches dimension size on the absorber were investigated. Three cases with different patches are depicted in Figure 9a. All of the patches in structures SO-I and SO-III had the same dimension size, while the dimension size of the patches in structure SO-II were different. The results in Figure 9b,c reveal that the patches with different dimension sizes improved the impedance matching around 6.5 GHz and slightly shifted the upper cutoff frequency higher.

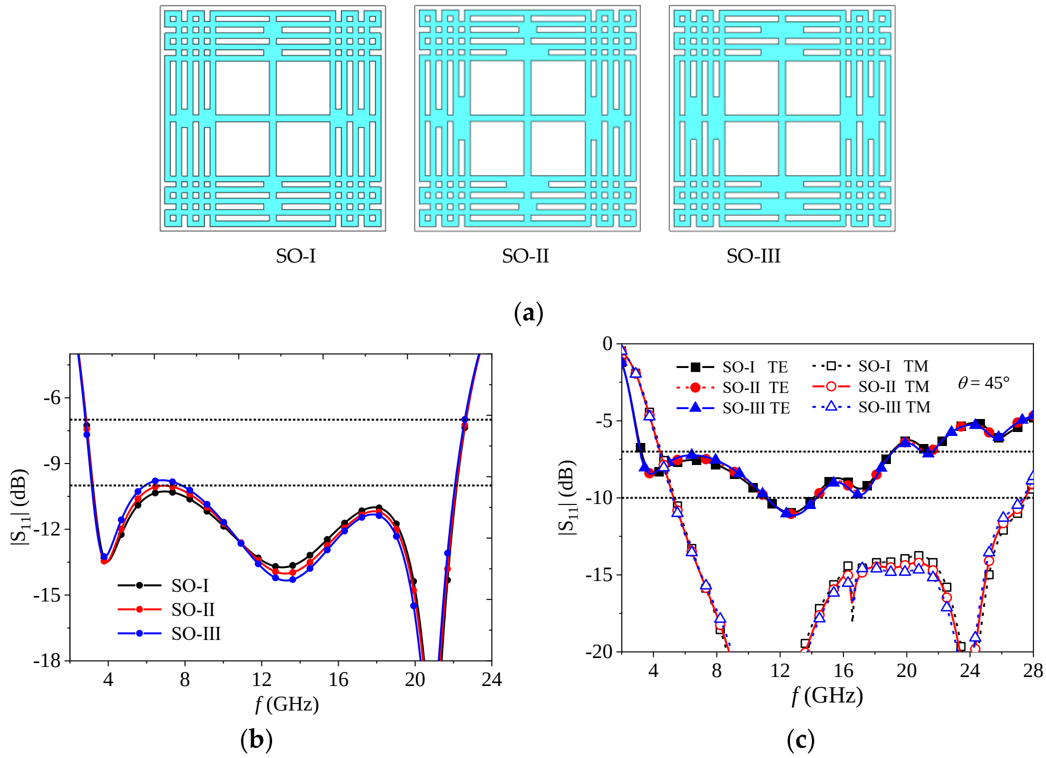

Figure 9. Effects of patches dimension size on the absorber. (**a**) Patches with different dimension size, and reflection coefficients of the absorber with different patches for normal (**b**) and oblique incidence at θ = 45° (**c**).

Finally, all the structural parameters of the final absorber structure (shown in Figure 1) were optimized by parameter-sweeping and listed in Table 1.

Table 1. Optimized parameters of the proposed FSS Absorber.

Parameters	Values (mm)	Parameters	Values (mm)
P	10	n	1.9
a	9.1	h_1	5.5
b	0.25	h_2	0.175
c	0.25	h_3	1
g	0.3	h_4	1.5
m	0.8	Sheet resistance	36 Ω/sq

3. Performance Evaluation of the Absorber

3.1. Angular Stability of the Absorber

Achieving incident angle stability and polarization insensitivity is crucial for the design of an effective microwave absorber. It is important to consider that electromagnetic waves can approach the absorber from various directions. Figure 10 shows the effect of different incidence angles on the absorptivity of the absorber in TE and TM polarization modes.

At normal incidence, the proposed FSS absorber demonstrated exceptional performance, achieving over 90% wave absorption within the frequency range of 3.1–22.1 GHz, with a relative bandwidth of 150.8% for both TE and TM polarizations. Further highlighting its robustness, the absorber maintained an absorptivity of more than 80% within the frequency range of 4.4–19.1 GHz, even under 45° oblique incidence, for both polarizations. In particular, for TM polarization waves, the absorber showed an absorption angle stability of 80% at up to 60°, while maintaining the bandwidth from 8.0 to 22.6 GHz. These results clearly demonstrate that the proposed absorber achieves excellent incident angle stability and polarization insensitivity across an ultrawide frequency range. It effectively absorbs incident waves regardless of the direction and polarization, making it highly suitable for diverse microwave applications.

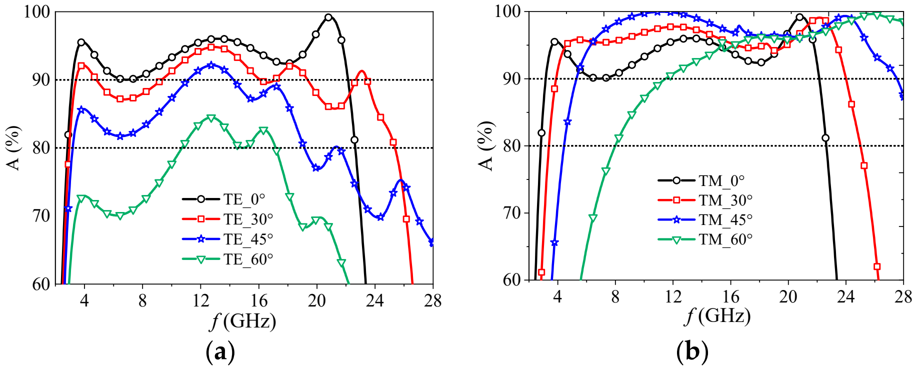

Figure 10. Absorption rate of the proposed absorber with respect to the incident angles for (**a**) TE polarizations (**b**) TM polarizations.

3.2. Effects of Sheet Resistance Fluctuation on the Absorber

Taking into account the inherent uncertainty associated with the sheet resistance (R_s) of a physical ITO material, which may vary due to processing and fabrication, its impact on the absorption rate was investigated, and results are shown in Figure 11. As the sheet resistance decreased from 36 Ω/sq to 26 Ω/sq, the absorption rate experienced a decline, falling below 90% but remaining above 80% within the frequency range of 4.2–9.9 GHz. However, it is important to note that the absorber maintained its exceptional performance, consistently achieving over 90% absorption beyond this band. Conversely, increasing the square resistance from 36 Ω/sq to 45 Ω/sq had a minimal effect on the absorber's 90% absorption bandwidth, which remained nearly unchanged. The remarkable characteristics of the proposed absorber lies in its ability to sustain at least 80% absorption even when confronted with significant sheet resistance fluctuations, ranging from 26 Ω/sq to 66 Ω/sq, across an ultrawide band spanning from 3.5 GHz to 22.4 GHz. This attribute holds remarkable importance in resistive film absorber design, as resistive film fabrication often leads to notable variations in sheet resistance within a relatively large range [22].

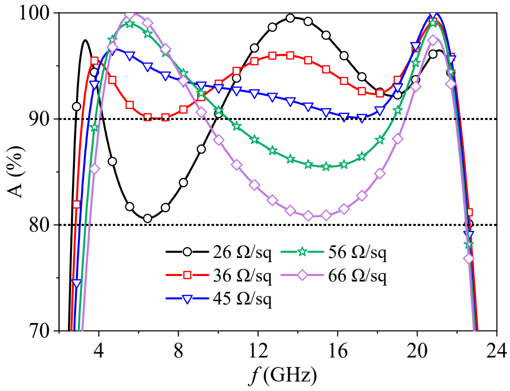

Figure 11. Absorption rate of the proposed absorber with respect to the sheet resistance (R_s).

3.3. Thickness of the Absorber

The thickness of the proposed absorber is 8.21 mm, about 0.085 λ_L. According to Rozanov's investigation, the theoretical minimum thickness of a nonmagnetic absorber is given as [19]

$$RL_h = \frac{\left|\int_0^\infty ln|S_{11}(\lambda)|d\lambda\right|}{2\pi^2} \quad (3)$$

where $|S_{11}(\lambda)|$ is the reflection coefficient as a function of wavelength. Using the reflection coefficient obtained, the minimum thickness of the absorber is about 7.60 mm. Thus, the overall thickness of the proposed absorber is approximately 1.08 times the theoretical limit, making it advantageous for applications with limited space or where a thinner design is desired.

4. Experiment Verification

To experimentally verify the absorber design, a prototype of 29 × 29 cells with dimensions of 300 mm × 300 mm × 8.21 mm was fabricated, as shown in Figure 12a. The measurement was conducted in an anechoic chamber, in accordance with the method described in [23], and the measurement setup is shown in Figure 12b. Two groups of wideband horn antennas were used to transmit and receive the signal. Those antennas were placed 1.5 m away from the absorber. The S-parameters were measured by an Agilent E8363C vector network analyzer.

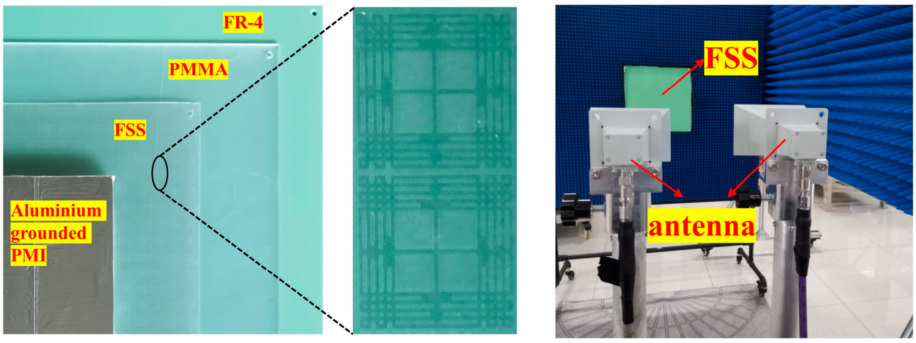

(**a**) (**b**)

Figure 12. The prototype of the absorber (**a**) and measurement setup (**b**).

The measured absorption rate in comparison with the simulation for normal incidence is illustrated in Figure 13a,b. Good agreements are observed between them. The measured 90% absorption bandwidth was 3.1–21.1 GHz with good polarization independence. The bandwidth shrinks by approximately 1.0 GHz more at a high frequency than the design, mainly due to the fabrication tolerance.

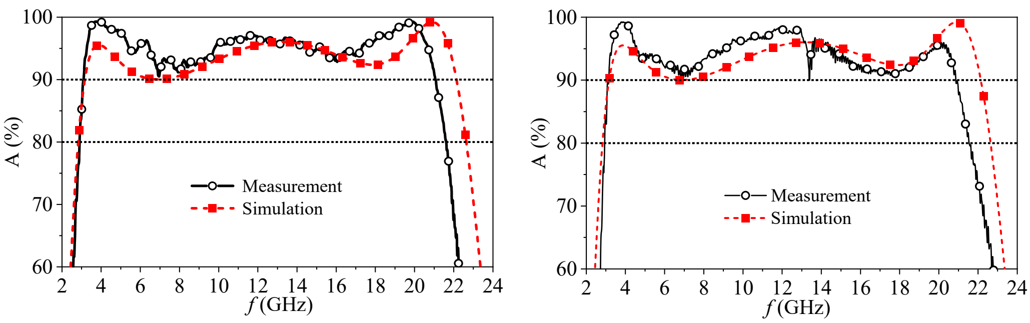

(**a**) (**b**)

Figure 13. Simulated and measured absorption rate under normal incidence for (**a**) TE and (**b**) TM polarizations.

Figure 14 depicts the measured absorption rate with respect to the incident angle for both TE and TM polarizations. It is evident that the measured 80% absorption rate covers a wide band of 4.4–20.3 GHz (128.7%) at an incident angle of θ = 45° for both TE and TM polarizations. In addition, the 80% absorption angular stability of TM polarization reached up to 60° while maintaining the broad bandwidth from 8.3 GHz to 21.5 GHz. The measured results are in good agreements with the simulations.

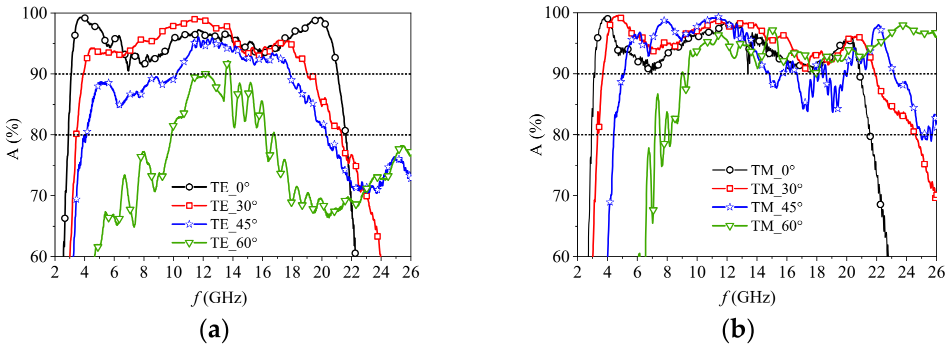

Figure 14. Measured absorption rate with respect to the incident angle for (**a**)TE and (**b**) TM polarizations.

The performance of the proposed absorber was compared with the related studies reported in the literature, as shown in Table 2. Compared to other single-layer FSS absorbers, the proposed absorber offers a wider bandwidth, reaching from 3.1 GHz to 22.1 GHz, with a fractional bandwidth of 150.8%. This expanded bandwidth allows for a more efficient absorption over a broader frequency range. In terms of thickness, the proposed absorber has a thickness of 0.085 λ_L, which is relatively thin compared to the absorbers utilizing multiple FSS layers. In summary, the proposed absorber exhibits significant advantages in terms of overall performance, including bandwidth, angular stability, and thickness, particularly when compared to absorbers that utilize only a single-FSS layer.

Table 2. Comparison between proposed and other FSS-based absorbers.

Ref.	BW (A $\geq$ 90%)	FBW(%)	Thickness (λ_L)	FSS Layer	Compensation Layer	Angular Stability/FBW (A $\geq$ 80%)
[11]	2.0–23.0	168.0%	0.10	3	-	45°/168.0%
[12]	2.8–20.6	152.0%	0.115	2	-	60°/130.0%
[13]	0.45–2.34	135.5%	0.069	1	no	30°/135.5%
[14]	4.0–17.2	124.5%	0.080	1	no	40°/110.0%
[15]	2.3–13.3	141.0%	0.138	1	yes	45°/107.5%
[17]	5.6–29.2	135.5%	0.091	1	yes	45°/135.5%
This work	3.1–22.1	150.8%	0.085	1	yes	45°/124.6%

5. Conclusions

This paper presents a novel single-layer FSS ultra-broadband thin absorber that exhibits remarkable performance in terms of angular stability, polarization insensitivity, and compactness. The designed FSS unit cell, consisting of a second-order Chinese knot and a cross, enables diverse current paths and multiple resonances in a wide frequency band. To enhance the absorber's performance, a compensation layer composed of FR4 and PMMA slabs with different thickness was added. This addition further improved the absorber bandwidth and angular stability.

The simulation results demonstrate the exceptional capabilities of the proposed absorber. It achieved an absorption rate exceeding 90% within the frequency range of 3.1–22.1 GHz, effectively covering the S to K-bands. Importantly, even when subjected to an oblique incidence of 45°, the absorber maintained an 80% absorption rate in the frequency range of 4.4–20.3 GHz for both TE and TM polarizations. The total thickness of the FSS absorber was 1.08 times the Rozanov limit, making it a compact design. A prototype of the proposed absorber has been fabricated and measured, showing good agreement with the simulation results. The comprehensive performance of the proposed absorber surpasses the related designs reported in the literature, offering comparable advantages.

Notably, it is possible to convert the proposed absorber into a transparent variant. This can be achieved by substituting the FR4 with PMMA material, replacing the PMI foam with air, and exchanging the metallic ground plate with an ITO film that possesses a small sheet resistance (e.g., 5 Ω/sq). Although the performance of the transparent absorber variant is slightly inferior to the original proposed absorber, its transformation opens up possibilities for diverse applications.

In summary, the compact size and exceptional performance of the proposed absorber make it a promising candidate for various applications, including electromagnetic interference suppression, radar cross-section reduction, and energy harvesting.

Author Contributions: Conceptualization, L.Y.; Formal analysis, C.Z. and L.Y.; investigation, C.Z., S.L. and H.N.; methodology, C.L. and L.Y.; validation, C.Z., S.L. and R.T.; writing—original draft, C.Z., R.T. and L.Y.; writing—review and editing, C.L. All authors have read and agreed to the published version of the manuscript.

Funding: This research was funded by National Natural Science Foundation of China, grant number U22A2015.

Data Availability Statement: All relevant data have been presented in article.

Acknowledgments: The authors would like to thank the graduate students Yushuang Jin, Xi Li and Wu Yang in Sichuan University for their kind help with experiments.

Conflicts of Interest: The authors declare no conflict of interest.

References

1. Hossain, M.I.; Nguyen-Trong, N.; Abbosh, A.M. Broadband Magnetic Absorber Based on Double-Layer Frequency-Selective Surface. *IEEE Trans. Antennas Propag.* **2022**, *70*, 410–419. [CrossRef]
2. Abidin, Z.U.; Cao, Q.; Shah, G. Design of a Compact Single-Layer Frequency Selective Surface with High Oblique Stability. *IEEE Trans. Electromagn. Compat.* **2022**, *64*, 2060–2066. [CrossRef]
3. Abdul Shukoor, M.; Dey, S. Broadband Polarization Insensitive Angular Stable Cross Dipole Loaded Circular Ring Circuit Analog Absorber (CAA) for X to K-Band Applications. In Proceedings of the 2020 International Symposium on Antennas & Propagation (APSYM), Cochin, India, 14–16 December 2020; pp. 97–100.
4. Sun, T.; Yin, F.; Xu, C.; Zhao, S.; Yan, H.; Yi, H. Ultrawideband Precision RCS Regulation for Trihedral Corner Reflectors by Loading Resistive Film Absorbers. *Electronics* **2022**, *11*, 3696. [CrossRef]
5. Decoster, B.; Maes, S.; Cuiñas, I.; García Sánchez, M.; Caldeirinha, R.; Verhaevert, J. Dual-Band Single-Layer Fractal Frequency Selective Surface for 5G Applications. *Electronics* **2021**, *10*, 2880. [CrossRef]
6. Farooq, U.; Iftikhar, A.; Shafique, M.F.; Khan, M.S. C-Band and X-Band Switchable Frequency-Selective Surface. *Electronics* **2021**, *10*, 476. [CrossRef]
7. Yang, Y.; Li, W.; Salama, K.N.; Shamim, A. Polarization Insensitive and Transparent Frequency Selective Surface for Dual Band GSM Shielding. *IEEE Trans. Antennas Propag.* **2021**, *69*, 2779–2789. [CrossRef]
8. Shi, C.; Zou, J.; Gao, J.; Liu, C. Gain Enhancement of a Dual-Band Antenna with the FSS. *Electronics* **2022**, *11*, 2882. [CrossRef]
9. Chakradhary, V.K.; Baskey, H.B.; Roshan, R.; Pathik, A.; Akhtar, M.J. Design of Frequency Selective Surface-Based Hybrid Nanocomposite Absorber for Stealth Applications. *IEEE Trans. Microw. Theory Tech.* **2018**, *66*, 4737–4744. [CrossRef]
10. Zheng, J.; Zheng, H.; Pang, Y.; Qu, B.; Xu, Z. Transparent broadband absorber based on a multilayer ITO conductive film. *Opt. Express* **2023**, *31*, 3731–3742. [CrossRef]
11. Gao, M.; Chen, Q.; Zheng, Y.; Ding, L.; Liao, D.; Fu, Y. Ultrabroadband Absorber Based on Layered Inkjet-Printing Resistive Film. *IEEE Antennas Wirel. Propag. Lett.* **2023**, *22*, 228–232. [CrossRef]
12. Sun, Z.; Yan, L.; Zhao, X.; Gao, R.X.-K. An Ultrawideband Frequency Selective Surface Absorber with High Polarization-Independent Angular Stability. *IEEE Antennas Wirel. Propag. Lett.* **2023**, *22*, 789–793. [CrossRef]
13. Cao, Z.; Yao, G.; Zha, D.; Zhao, Y.; Wu, L.; Miao, L.; Bie, S.; Jiang, J. Impedance Well Effect from Circuit Analysis and New Design Concepts for Ultrabroadband Passive Absorber. *IEEE Trans. Antennas Propag.* **2022**, *70*, 9942–9946. [CrossRef]
14. Sheokand, H.; Singh, G.; Ghosh, S.; Ramkumar, J.; Ramakrishna, S.A.; Srivastava, K.V. An Optically Transparent Broadband Microwave Absorber Using Interdigital Capacitance. *IEEE Antennas Wirel. Propag. Lett.* **2019**, *18*, 113–117. [CrossRef]
15. He, F.; Si, K.; Li, R.; Zha, D.; Dong, J.; Miao, L.; Bie, X.; Jiang, J. Broadband Frequency Selective Surface Absorber with Dual-Section Step-Impedance Matching for Oblique Incidence Applications. *IEEE Trans. Antennas Propag.* **2021**, *69*, 7647–7657. [CrossRef]

16. He, F.; Si, K.; Zha, D.; Li, R.; Zhang, Y.; Dong, J.; Miao, L.; Bie, S.; Jiang, J. Broadband Microwave Absorption Properties of a Frequency-Selective Surface Embedded in a Patterned Honeycomb Absorber. *IEEE Trans. Electromagn. Compat.* **2021**, *63*, 1290–1294. [CrossRef]
17. Zhao, Y.; Li, S.; Jiang, Y.; Gu, C.; Liu, L.; Li, Z. An ultra-wideband and wide-angle optically transparent flexible microwave metamaterial absorber. *J. Phys. D Appl. Phys.* **2021**, *54*, 275101. [CrossRef]
18. Chen, J.; Ding, W.; Li, X.; Xi, X.; Ye, K.; Wu, H.; Wu, R. Absorption and Diffusion Enabled Ultrathin Broadband Metamaterial Absorber Designed by Deep Neural Network and PSO. *IEEE Antennas Wirel. Propag. Lett.* **2021**, *20*, 1993–1997. [CrossRef]
19. Rozanov, K.N. Ultimate thickness to bandwidth ratio of radar absorbers. *IEEE Trans. Antennas Propag.* **2000**, *48*, 1230–1234. [CrossRef]
20. CST Studio Suite 3D EM Simulation and Analysis Software. Available online: https://www.3ds.com/products-services/simulia/products/cst-studio-suite/ (accessed on 1 November 2020).
21. Kazemzadeh, A.; Karlsson, A. Multilayered Wideband Absorbers for Oblique Angle of Incidence. *IEEE Trans. Antennas Propag.* **2010**, *58*, 3637–3646. [CrossRef]
22. Kazemzadeh, A. Nonmagnetic Ultrawideband Absorber with Optimal Thickness. *IEEE Trans. Antennas Propag.* **2011**, *59*, 135–140. [CrossRef]
23. Yao, Z.; Xiao, S.; Wang, B. Study on an Accurate and Efficient Design Method of Resonant FSSs Based on the Macro-Model of Units in the Basic Strip-Gap FSS. *IEEE Trans. Antennas Propag.* **2021**, *69*, 2741–2750. [CrossRef]